http://dx.doi.org/10.21577/0103-5053.20190146

J. Braz. Chem. Soc., Vol. 30, No. 11, 2367-2375, 2019
Printed in Brazil - ©2019 Sociedade Brasileira de Química

Article

Experimental and Computational Studies of the Adsorption of Furan, Pyrrole, and Thiophene on Hydroxyapatites in a Single and Ternary Component

Mayara S. Oliveira,[,a,b] Stefane N. Costa,[b] Norberto K. V. Monteiro,[b] Pedro L. Neto,[b] Guilherme A. Magalhães Junior,[a] Izaura C. N. Diógenes,[c] Rinaldo S. Araújo[d] and Elisane Longhinotti*[,b]*

[a]*Instituto Federal de Educação, Ciência e Tecnologia do Ceará, Campus Quixadá, 63902-580 Quixadá-CE, Brazil*

[b]*Departamento de Química Analítica e Físico-Química, Universidade Federal do Ceará, 60455-970 Fortaleza-CE, Brazil*

[c]*Departamento de Química Orgânica e Inorgânica, Universidade Federal do Ceará, 60455-970 Fortaleza-CE, Brazil*

[d]*Instituto Federal de Educação, Ciência e Tecnologia do Ceará, Campus Fortaleza, 60040-531 Fortaleza-CE, Brazil*

Non-doped (Hap) and doped hydroxyapatites with Cu^{2+} and Fe^{2+} were synthesized and used to study the adsorption of furan (Fur), pyrrole (Pyr), and thiophene (Thi) in single and ternary component systems. Spectroscopic data and N_2 isotherms indicated there were no structural alterations in Hap with the incorporation of Cu^{2+} and Fe^{2+}. For both single and ternary components, the incorporation of the metal ions resulted in an adsorption increment consistent with the hard-soft acid-base concept. When comparing the systems, there is an inversion with Thi (5.41 mg g^{-1}) and Fur (5.51 mg g^{-1}) being the most adsorbed species in the single and ternary components, respectively. Monte Carlo simulations helped explain the observed experimental trends. While the electrostatic effect seems to prevail in the single system, in the ternary one the mass transport phenomenon is also operative implying greater availability of Fur on surface leading to its higher adsorption efficiency.

Keywords: hydroxyapatite, adsorption, aromatic heterocyclic, Monte Carlo

Introduction

Nitrogen oxides (NOx) and sulfur oxides (SOx), emitted from stationary and mobile sources, remain to be important sources of air pollution, because they contribute to acid rain, ozone depletion, greenhouse effects, etc. Thus, with increasingly strict regulations on air pollutant emissions,[1] heterocyclic organic molecules such as furan (Fur), pyrrole (Pyr) and thiophene (Thi) obtained from petrochemical chains are also worth mentioning because they are related to health and environmental problems. Investigations on alternative ways for reducing sulfur, nitrogen and oxygen of fuels, using several materials as adsorbents, with special attention to environmentally friendly, biocompatible and low-cost materials have been continuously performed by the scientific community.[2-13] Among these materials, hydroxyapatite (Hap, $Ca_{10}(PO_4)_6(OH)_2$) has been used for the purpose of soil[14-16] and water decontamination.[17-19] This compound, which is a natural form of calcium apatite, has been widely used as alternative in applications such as bioceramic,[20] catalyst,[21] and adsorbent[5,17,19] due to its interaction with several cations and anions in the ionic adsorption/exchange process.[22] In addition, because of the excellent stability, hydroxyapatite easily accepts ionic substituents in its structure. For instance, Ca^{2+} cations in the Hap structure can be substituted by a given ion though limited by the size of ions and Ca/metal molar ratio.[23] The vacancies created as result of the substitution help in tailoring the properties of Hap as adsorbent.[24] In this context, theoretical studies including Monte Carlo (MC) simulations have been performed in adsorption studies to shed light on the understanding of the process in a

*e-mail: mdsoliveira24@gmail.com; elisane@ufc.br

molecular level.[25-28] A few theoretical studies,[29] however, have been found on the adsorption on Hap surface making this issue an open avenue to understanding the atomistic structural aspects of this specific process.

In this work, hydroxyapatites doped with Cu^{2+} (HapCu) and Fe^{2+} (HapFe) were prepared and used as adsorbents for three heterocyclic molecules, pyrrole, furan, and thiophene in single and ternary component systems. All measurements were performed in pure isooctane intending to mimic the condition found in fuels. Aiming to get insights on the adsorption behavior of these heterocyclic compounds on Hap, Monte Carlo simulations were performed focusing on the most stable adsorption configurations thus providing support for the understanding of the molecular structural aspects that drive the control and performance of hydroxyapatites toward a specific application.

Experimental

Chemicals

H_3PO_4 (85%), $CaCl_2.2H_2O$ (99%), $Cu(NO_3)_2.3H_2O$ (98%), $Fe(NO_3)_2.9H_2O$ (99%), and isooctane (99.5%), purchased from Vetec, and furan (Fur, 99.0%), pyrrole (Pyr, 98.0%), and thiophene (Thi, 99.0%), purchased from Sigma-Aldrich (Saint Louis, USA), were used as received. Aqueous solutions were prepared using water purified in Direct Q® 3UV water purification system (Merck Millipore) with resistivity greater than 18.2 MΩ cm at 25 °C.

Synthesis and characterization of adsorbents

Pure hydroxyapatite (Hap, $Ca_{10}(PO_4)_6(OH)_2$) was synthesized as described in the literature[30] with minor modifications. In brief: 100 mL of 0.3 mol L^{-1} H_3PO_4 was slowly dropped to a beaker containing 100 mL of 0.5 mol L^{-1} $CaCl_2.2H_2O$ (molar ratio Ca/P = 1.67) under continuous stirring at room temperature. The pH was adjusted to ca. 9.5 by adding 0.5 mol L^{-1} NaOH to force the precipitation. Same protocol was followed for the synthesis of HapCu and HapFe with the addition of 10 mmol of $Cu(NO_3)_2.3H_2O$ and 6 mmol of $Fe(NO_3)_2.9H_2O$, respectively, just before the pH raise. The obtained solid products were filtered, washed, dried at 60-70 °C for 24 h and calcined at 550 °C for 3 h in air.

Attenuated total reflectance-Fourier transform infrared (ATR-FTIR) spectra were acquired using a Spectrum 100 FT-IR (PerkinElmer) spectrometer with a 4 cm^{-1} of resolution, coupled to MIRacle ATR from Pike Technologies. The spectra were collected using 20 scans min^{-1}.

X-ray diffraction (XRD) analyses for Hap, HapFe, and HapCu were performed with a DMAXB-Rigaku diffractometer using a Cu Kα radiation source (λ = 1.5405 Å), 40 kV, 25 mA and 2θ from 10° to 90° at room temperature.

The amounts of Ca^{2+}, Cu^{2+}, and Fe^{2+} in the prepared hydroxyapatites were determined by flame atomic absorption spectroscopy (FAAS) using an iCE 3000 from Thermo Scientific (analyses conditions listed in Table S1, Supplementary Information (SI) section) with limit of detection (LOD) of 0.033 μg mL^{-1}. The analyzes, run in duplicate, were carried out by acid digestion of 100 mg of the adsorbents in 10 mL of aqua regia.

The amount of phosphorus was spectrophotometrically determined according to the colorimetric methodology (4500-P E, ascorbic acid method) described in APHA[31] using a Spectrophotometer Thermo Scientific Evolution 60S with xenon lamp and double silicon photodiode detector operating in the ultraviolet and visible regions (UV-Vis) by following the absorbance changes of the absorption at 880 nm.

Nitrogen adsorption/desorption isotherms were carried out in a Quantachrome Autosorb-1B instrument at 77 K. The samples were degassed at 523 K under vacuum for 12 h prior to the measurement. The specific surface area of the samples was calculated using the Brunauer-Emmett-Teller (BET) method.[32] The pore size distribution was derived from the adsorption branches of the isotherms using the Barrett-Joyner-Halenda (BJH) method.

Zeta potential values (ζ, mV) were measured in triplicate in aqueous suspension at 1.0% m/v (pH 7) by using a Zetasizer Nano ZS (Malvern Instruments Ltd.).

Adsorption experiments

Typically, batch adsorption experiments were conducted in triplicate to determine the adsorption capabilities of Hap, HapCu and HapFe samples for thiophene (Thi), pyrrole (Pyr) and furan (Fur) adsorbates using isooctane as solvent. The experiments were carried out using solutions prepared by the dispersion of 200 mg of adsorbents into 25 mL of the adsorbate solutions (10-100 mg L^{-1}). The samples were equilibrated on a shaker for 8 h at 150 rpm with temperature at 25 °C followed by centrifugation for 10 min to separate the adsorbents. The concentrations of furan, pyrrole, and thiophene were determined by injecting 10 μL in a Thermo Scientific UHPLC ACCELA system equipped with a Hypersil Gold (C18) (50 cm × 2.1 mm, 3.0 μm) and a UV-Vis detector (detection wavelength: λ = 220-230 nm). The obtained chromatograms are illustrated in Figure S1a (SI section). The mobile phase consisted of acetonitrile/water (50% v/v) running at 300 μL min^{-1}. For the kinetics

studies, 50 mg L^{-1} of the adsorbates was used as initial concentration. The adsorption amount (qt, in mg g^{-1}) of the adsorbates were calculated by the following mass balance relationship: $qt = \frac{(C_o - C_t)V}{W}$, where C_o and C_t are the initial and final (at a time t) concentrations of the adsorbates in solution (mg L^{-1}), respectively, V is the volume (in L) and W is the mass (g) of the adsorbents. The concentration of adsorbates in the solution (C_t) was calculated at equilibrium and designated as C_e (mg L^{-1}). For the analytical curves, working solutions of the heterocyclic aromatic standard mixture, ranging from 0.5 to 15 mg L^{-1}, were prepared by dilution from 1000 mg L^{-1} stock solution in isooctane (Figure S1b, SI section).

Computational details

The geometry optimization calculations were performed by using a hybrid generalized gradient approximation functional B3LYP[33-35] with the 6-31G(d,p) basis set by using the Gaussian 09 package.[36] Frequency calculations were performed to analyze vibrational modes of the optimized geometries in order to determine whether the resulting geometries are true minima or transition states.

Quantum chemical methods have a particular importance in understanding the stability and reactivity of molecules.[37-39] From the work of Parr and co-workers,[35] useful concepts have been derived from the electron density of molecular systems through density functional theory (DFT) which is based on the Kohn-Sham theory.[40] These concepts allow to obtain quantitative data about the reactivity of molecular systems and are collectively known as conceptual DFT descriptors.[41]

Frontier molecular orbitals (HOMO (highest occupied molecular orbital) and LUMO (lowest unoccupied molecular orbital)) were determined to predict the reactivity of the studied species.[37] The HOMO orbital energy (E_{HOMO}) is normally related to the electron-donating ability of a molecule whereas LUMO orbital energy (E_{LUMO}) is associated with the electron-accepting ability of a molecule from which the global hardness (η) can be calculated. Following the Janak's[40] theorem, this parameter is determined in terms of the ionization potential (I) and the electron affinity (A) as $\eta = \frac{I - A}{2}$, while the softness, the inverse of the hardness, is calculated as $\sigma = \frac{1}{\eta}$. According to the Koopmans' theorem,[41] ionization potential can be estimated as the negative of the HOMO energy, $I = -E_{HOMO}$, and electron affinity as the negative of the LUMO energy, $A = -E_{LUMO}$.

The Monte Carlo method[42] allows to calculate the position and orientation of a molecule on a fixed substrate as well as the energy of interaction. Based on this method, the Adsorption Locator program implemented in the Material Studio 8.0 package[43] was used to calculate the interaction energies of the pyrrole, furan and thiophene molecules in isooctane solvent on the Hap surface. Before the simulations, the Hap plane (001) was cleaved from the crystal of the Hap,[44] expanded to a super cell ($3 \times 3 \times 1$) and, finally, to a vacuum plate with a thickness of 30 Å where the Hap plane (001) was constructed. We used the ultrafine quality Dreiding force field[45] with the following parameters: 2×10^{-5} kcal mol^{-1} of energetic variation, 10^{-3} kcal mol^{-1} Å of maximum force variation and 1×10^{-5} Å of maximum displacement in the cartesian coordinates. For the execution of the calculation, 45 molecules of the isooctane solvent and the molecules of pyrrole, furan and thiophene were inserted individually (single component) and mixed (ternary component) in the system.

Results and Discussion

Synthesis and characterization of adsorbents

The synthesized hydroxyapatites doped with Cu^{2+} (HapCu) and Fe^{2+} (HapFe) were characterized by FAAS, ATR-FTIR, XRD, and N_2 isotherms and the data were evaluated in comparison to the non-doped Hap material.

The amounts of metals incorporated in the hydroxyapatites, determined by FAAS, indicate ca. 6.3 and 5.5% of Cu and Fe in HapCu and HapFe, respectively, thus corresponding to a Ca/metal molar ratio of about 9. The Ca/phosphorous (Ca/P) molar ratios were found as ca. 1.67 ± 0.02 for all the synthesized adsorbents indicating the hydroxyapatite structure was maintained and the preparation method was successfully applied. The ATR-FTIR spectra of Hap, HapCu, and HapFe (Figure S2, SI section) show the characteristic bands of Hap in the range from 1090 to 1033 cm^{-1} assigned to the asymmetric stretching modes of the P–O bond of PO_4^{3-} while the symmetric stretching and bending modes are observed at ca. 960 cm^{-1} and in the range from 600 to 470 cm^{-1}, respectively. The broad band observed above 3000 cm^{-1} is assigned to the stretching modes of the OH bond of water and phosphate groups.[17,20,30,46] No significant change was observed in the ATR-FTIR spectra of the HapCu and HapFe suggesting the incorporation of the metallic ions did not alter the hydroxyapatite structure thus reinforcing the FAAS results. The XRD patterns shown in Figure S3 (SI section) present the diffraction lines corresponding to the hexagonal hydroxyapatite (PDF Ref. 09-0432) indicating

no meaningful structural changes in the hydroxyapatite have occurred upon the incorporation of the metal ions corroborating the FTIR suggestion. N_2 isotherms of Hap, HapCu, and HapFe (Figure S4, SI section) present similar profiles consistent with type II with a weak H3 hysteresis loop, according to the IUPAC classification.[47] The hysteresis type H3, in turn, is attributed to plate-shaped aggregates which give rise to slit-shaped pores corroborating the above results that pointed out for the typical hydroxyapatite morphology.[48] The textural parameters determined from the N_2 isotherms are summarized in Table 1.

In comparison to the non-doped Hap (41 $m^2 g^{-1}$), there is an increment in the surface areas after incorporation of Cu^{2+} (HapCu: 69 $m^2 g^{-1}$) and Fe^{2+} (HapFe: 64 $m^2 g^{-1}$). Such behavior has been frequently reported in the literature[49] being assigned to the decrease of the crystal size due to the incorporation of metal ions of lower ionic radius, i.e., in this work Fe^{2+} (0.77 Å) and Cu^{2+} (0.72 Å). The values of surface area fall within the range 31-52 $m^2 g^{-1}$ commonly reported for materials synthesized without structural directing agents, such as hydrothermal and sol-gel procedures.[50] The pore diameter, on the other hand, shows virtually no change (ca. 160 Å) indicating that the original pore structure of the hydroxyapatite is not meaningfully affected by the incorporation of the metal ions.

Adsorption experiments

The kinetic data of the adsorption process of Thi, Pyr and Fur on Hap, HapFe, and HapCu were evaluated in single and ternary component systems assuming the intraparticle diffusion, pseudo-first- and pseudo-second-order models. For the determination of the maximum adsorption capacity (q_{max}) of the adsorbents, Langmuir, Freundlich, and Sips isotherm models were applied to the experimental data (all model's equations are given in Table S2, SI section). For the sake of simplicity, Figure 1 presents the kinetic and isotherm curves only for the adsorption of Thi, Pyr and Fur on Hap since all adsorbents presented very similar behavior. The kinetic curves and isotherms for HapFe and HapCu for single and ternary component systems are shown in Figures S5 to S8 (SI section).

Curves a and b of Figure 1 show the saturation of the adsorbent occurs after 500 min for both the single and ternary components, although with different values of adsorption capacity at the equilibrium (q_e), as can be seen in Table 2. The kinetic parameters were estimated by nonlinear method using the expressions of kinetic models given in Table S2 (SI section). The best fit of the experimental q_e values was found by using the pseudo-first-order model indicating the adsorption of Fur, Pyr, and Thi can be well-represented by this model from which the theoretical values of adsorption capacity at the equilibrium (q_{e1}) were estimated (Table 2).

If assuming the intraparticle diffusion model, a plot of the square root of time ($t^{0.5}$) *versus* qt must result in a linear relation passing through the origin.[51] For the studied materials, multilinear plots (Figure S9, SI section) were observed suggesting a more complex mechanism should be considered for explaining the adsorption of the five-membered heterocyclic Fur, Pyr, and Thi molecules on the Hap, HapFe, and HapCu adsorbents.

The adsorption isotherms shown in Figure 1 (c and d) indicate different trends when applying single and ternary component systems. For the latter one, the higher adsorption efficiency was observed for furan while thiophene was the most adsorbed molecule in the single component system. The thermodynamic experimental data were treated with Langmuir, Freundlich, and Sips models being best fitted to the Langmuir and Sips models. The adsorption parameters estimated from these models are summarized in Table S3 (SI section).

For both single and ternary component systems, the experimental values of maximum adsorption capacity, $q_{max(exp)}$, of all adsorbates increased upon the metal ions incorporation; e.g. 6.27 ± 0.079 mg g^{-1} and 6.42 ± 0.094 mg g^{-1} for the adsorption of Fur on HapFe and HapCu, respectively, in comparison to 4.05 ± 0.053 mg g^{-1} for Hap in the ternary component system (Table S3, SI section). This behavior can be firstly explained based on the well-known hard-soft acid-base (HSAB) concept of Pearson.[52] Accordingly, soft-soft and hard-hard interactions are stronger than hard-soft ones. Due to the high π electron density of Fur, Pyr, and Thi, these molecules

Table 1. Chemical composition and textural properties for the hydroxyapatite adsorbents

Adsorbent	Metal[a] / wt.%	Ca/metal molar ratio	Ca/P molar ratio	S_{BET}[b] / ($m^2 g^{-1}$)	d_{pore}[c] / Å	V_{pore} / ($cm^3 g^{-1}$)
Hap	–	–	1.68	41	159	0.72
HapFe	5.5	9	1.67	64	162	0.69
HapCu	6.3	9	1.67	69	161	0.85

[a]Flame atomic absorption spectroscopy (FAAS); [b]superficial area calculated by Brunauer-Emmett-Teller (BET) method; [c]pore diameter calculated by Barrett-Joyner-Halenda (BJH) method. Hap: hydroxyapatite.

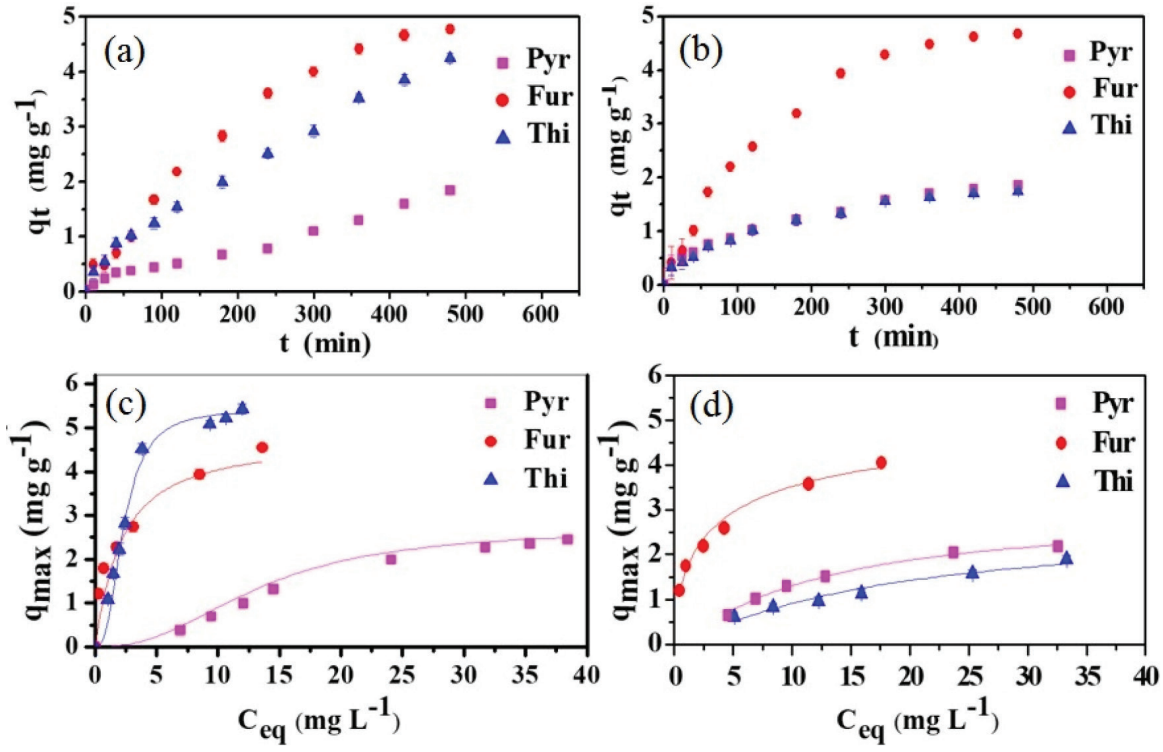

Figure 1. Kinetic plots (a, b) and isotherms (c, d) at 298 K for single (a, c) and ternary (b, d) components for the adsorption of Thi, Pyr, and Fur on Hap. Solid lines in plots c and d shows the trend of the data and not the fit.

Table 2. Kinetic parameters for the adsorption of Fur, Pyr, and Thi on the synthesized hydroxyapatites using the pseudo-first order model in single and ternary component systems

System	Adsorbent	Adsorbate[a]	q_e / (mg g^{-1})	q_{e1} / (mg g^{-1})	k_1 / min^{-1}	SSRE	R^2
Single	Hap	Thi	5.13	5.67	0.0052	0.011	0.996
		Fur	4.77	5.04	0.0052	0.003	0.987
		Pyr	2.12	2.32	0.0044	0.009	0.949
	HapFe	Thi	6.28	6.55	0.0062	0.002	0.989
		Fur	6.13	6.36	0.0055	0.001	0.994
		Pyr	3.86	4.07	0.0050	0.003	0.947
	HapCu	Thi	6.80	6.67	0.0089	0.000	0.965
		Fur	6.43	6.52	0.0061	0.000	0.968
		Pyr	4.30	4.46	0.0053	0.001	0.979
Ternary	Hap	Thi	1.75	1.80	0.005	0.001	0.973
		Fur	4.68	4.84	0.0063	0.001	0.976
		Pyr	1.86	1.89	0.006	0.000	0.981
	HapFe	Thi	2.22	2.31	0.0054	0.002	0.981
		Fur	5.64	5.63	0.0064	0.000	0.966
		Pyr	2.95	2.87	0.010	0.001	0.964
	HapCu	Thi	2.16	2.33	0.0056	0.006	0.978
		Fur	5.80	5.72	0.009	0.000	0.976
		Pyr	3.27	3.01	0.012	0.006	0.969

[a]Initial concentration of the adsorbate (C_0) = 50 mg L^{-1}. q_e: adsorption capacity at the equilibrium; q_{e1}: theoretical adsorption capacity at the equilibrium; k_1: first order rate constant; SSRE: sum of squares of relative error; R^2: coefficient of determination; Hap: hydroxyapatite; Thi: thiophene; Fur: furan; Pyr: pyrrole.

are considerable soft thus favoring interactions with the softer acids Cu^{2+} and Fe^{2+} whose hardness (η) is 8.27 and 7.24, respectively, in respect to Ca^{2+} (η = 19.52). It is worth mentioning that the softness of Cu^{2+} and Fe^{2+} is related to the electron population of d-orbitals, a feature that has been used to explain the π complexation of heterocyclic aromatics with metal ions.[53]

The adsorption studies performed for the ternary system showed other effects must be taken into account to explain the preferential adsorption of Fur on all the adsorbents, as clearly seen in Figures 1b and 1d. A reasonable hypothesis for this behavior laid on the different mass transport properties of each adsorbate in the solvent used in this work (isooctane). To further understand this issue, Monte Carlo simulations were performed focusing on the electronic parameters that affect the adsorption efficiency of the aromatic molecules on Hap.

Computational studies

Prior to the discussion of Monte Carlo simulations, which give a classical statistical treatment on the adsorption results, DFT calculations, a quantum mechanical approach, were performed in this work to generate the graphic distribution of HOMO and LUMO frontier orbitals (Figure 2a) of the studied adsorbate molecules. The quantum chemical parameters obtained are displayed in Table 3.

E_{HOMO}, E_{LUMO}, I, A, η and σ can be associated with the adsorption efficiency.[54] When comparing the HOMO and LUMO energy gap (ΔE), Figure 3, with the adsorption efficiencies determined for the single component system, Fur (q_{max} = 4.75 mg g^{-1}) and Thi (q_{max} = 5.41 mg g^{-1}) present lower values (ΔE = 6.639 and 6.122 eV, respectively) than that calculated for Pyr (q_{max} = 2.69 mg g^{-1}), 6.830 eV.

Knowing that the lower the energy gap, the higher it is the softness (σ) of a given species, the values of ΔE shown in Figure 3 are consistent with the calculated σ values for the aromatic molecules as given in Table 3. Having in mind that the Lewis acid of Hap, Ca^{2+}, is classified as a hard acid, it would be expected that Pyr (η = 3.415), the hardest studied adsorbate, would present the higher value

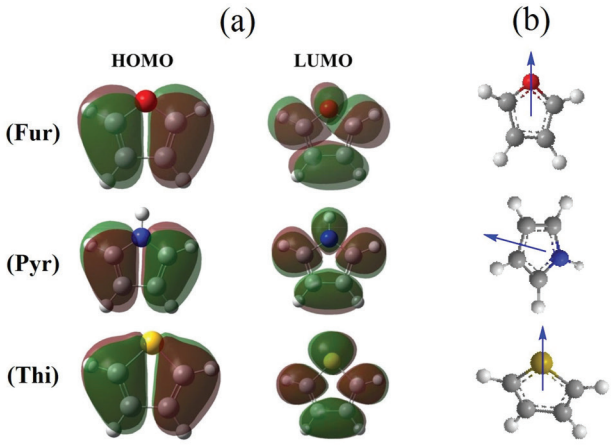

Figure 2. Calculated HOMO and LUMO frontier orbitals (a) and dipole vectors (b) for Fur, Pyr, and Thi.

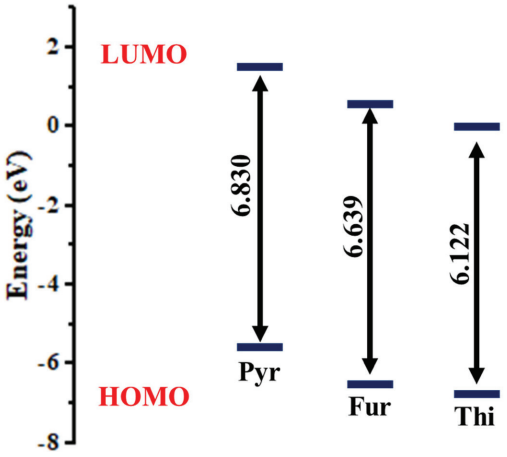

Figure 3. Plot of energy gap (ΔE) of HOMO and LUMO frontier orbitals for Pyr, Fur and Thi.

of adsorption efficiency. However, the calculated values point for an inverted trend with the softest molecules Thi and Fur presenting the higher values of q_{max}. It is evident, therefore, that factors other than acid-base interactions are operative in the studied adsorption process. In structures such as hydroxyapatites, the influence of the chemical environment surrounding the central cation cannot be ruled out. Indeed, hydroxyapatites have been frequently used to adsorb positively charged metals and proteins due to the negative charged phosphate groups surrounding the central

Table 3. Calculated quantum chemistry descriptors for Fur, Pyr, and Thi by using B3LYP at the 6-31G(d,p) basis set

Molecule	E_{HOMO} / eV	E_{LUMO} / eV	ΔE / eV	I / eV	A / eV	η / eV	σ	μ / Debye
Fur	–6.122	0.517	6.639	6.122	–0.517	3.320	0.301	0.627
Pyr	–5.497	1.333	6.830	5.497	–1.333	3.415	0.293	1.904
Thi	–6.340	–0.218	6.122	6.340	0.218	3.061	0.327	0.623

E_{HOMO}: highest occupied molecular orbital (HOMO) orbital energy; E_{LUMO}: lowest unoccupied molecular orbital (LUMO) orbital energy; ΔE: energy gap; I: ionization potential; A: electron affinity; η: global hardness; σ: global softness; μ: dipole moment; Fur: furan; Pyr: pyrrole; Thi: thiophene.

Ca^{2+} cation.[55-57] Based on the values of dipole moment calculated by DFT and displayed in Table 3, it seems the electrostatic effect prevails over the acid-base affinity for the non-doped hydroxyapatite. To further understand this behavior, Monte Carlo simulations were performed for the adsorption of Thi, Fur and Pyr on Hap. For the single component, the most stable adsorption configurations calculated by Monte Carlo (Figures 4a to 4c) were found when Thi adsorbs through S, Fur nearly parallel (with O slightly far apart from the surface) and Pyr perpendicular with the N atom on the opposite side of the surface.

As seen in Figure 4, the mean centroid-surface distances were calculated as 7.080, 4.140, and 5.267 Å for Fur, Pyr, and Thi, respectively, in the single component system. As indicated in Table 4, Pyr, although being the molecule nearest the surface, presents the lowest interaction energy (−19.917 kcal mol^{-1}). For the ternary component system, similar trend was observed for the mean centroid-surface distances, i.e., 7.475, 3.770, and 6.271 Å for Fur, Pyr, and Thi, respectively.

Considering the ζ of Hap in powder was determined as −18.7 ± 0.586 mV, the electrostatic effect seems, indeed, to prevail in explaining the observed trend Thi > Fur > Pyr. The vectors (Figure 2b) of the magnetic dipole moments of Thi (0.623 D), Fur (0.627 D), and Pyr (1.904 D) point for sulfur, oxygen and carbon atoms, respectively, showing the electrostatic repulsion drives the configuration and adsorption efficiencies of the studied heterocyclic aromatics molecules on Hap, as can be deduced from the data displayed in Table 4.

For the ternary component system (Figure 4d), the most stable configurations were reached when all aromatic

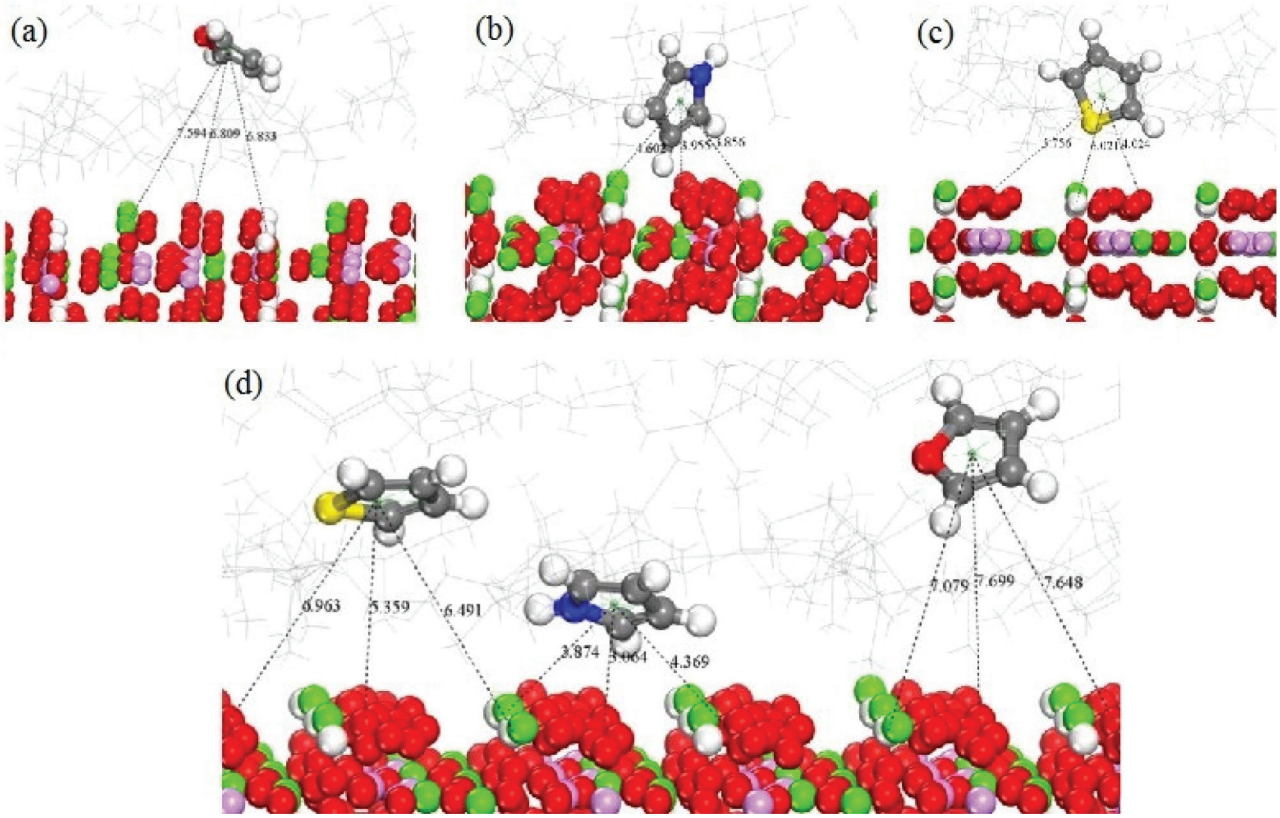

Figure 4. Preferred orientations of (a) Fur; (b) Pyr; and (c) Thi in the single component and (d) Fur + Pyr + Thi in the ternary component systems for the surface of Hap (001) and in the presence of isooctane solvent by using the Dreiding force field. The centroid-surface distances of the species studied are shown by dotted lines.

Table 4. Average of the Monte Carlo adsorption energies for the single component ($\underline{E}_{SC}$) and ternary component ($\underline{E}_{TC}$) systems

Molecule	$\underline{E}_{SC}$ / (kcal mol^{-1})	q_{max}[a] / (mg g^{-1})	$\underline{E}_{TC}$ / (kcal mol^{-1})	q_{max}[a] / (mg g^{-1})
Fur	−22.657	4.75	−24.094	5.51
Pyr	−19.917	2.69	−19.490	2.94
Thi	−23.841	5.41	−20.512	2.61

[a]Sips isotherm model (Table S3, SI section). q_{max}: maximum adsorption capacity; Fur: furan; Pyr: pyrrole; Thi: thiophene.

molecules adsorb parallel to the Hap surface. In such condition, besides the electrostatic effect, the mass transport phenomenon must be taken into account. As shown in Figure S10 (SI section) and Table 4, considering the interaction with the solvent molecules, the most negative value of energy is observed for Fur meaning its diffusion is favored in isooctane in comparison to Pyr and Thi. This physical aspect results in a greater availability of Fur on Hap surface leading to a higher adsorption efficiency. Therefore, the inversion in the adsorption efficiency values observed experimentally (Figure 1 and Table 4) for the ternary (Fur > Pyr ≅ Thi) in comparison to the single (Thi > Fur > Pyr) component system is well correlated with the calculated average adsorption energies.

Conclusions

The adsorption of the heterocyclic aromatic molecules furan (Fur), pyrrole (Pyr), and thiophene (Thi) on non-doped (Hap) and doped hydroxyapatites with Cu^{2+} (HapCu) and Fe^{2+} (HapFe) was experimentally and theoretically studied in single and ternary component systems. For both single and ternary component systems, the incorporation of the Cu^{2+} and Fe^{2+} ions resulted in an adsorption increment consistent with the hard-soft acid-base concept of Pearson. The softness of Cu^{2+} and Fe^{2+} due to the electron density of the d-orbitals favors the interaction with the soft bases Fur, Pyr, and Thi thus explaining such increment. Comparing the adsorption efficiencies, it was observed an inversion behavior with Thi being the most and less adsorbed species in the single and ternary component systems, respectively. The theoretical preferred orientations and energies of adsorption of Fur, Pyr, and Thi on Hap helped explain the experimental trends; Thi > Fur > Pyr and Fur > Pyr ≅ Thi for the single and ternary systems, respectively. For the single component, the most stable adsorption configurations were found when Thi adsorbs through S, Fur nearly parallel (with O slightly far apart the surface) and Pyr perpendicular with the N atom on the opposite side of the Hap surface.

For the non-doped hydroxyapatite, the electrostatic effect seems to prevail in explaining the observed trend since the vectors of the magnetic dipole moments of Thi, Fur, and Pyr point for sulfur, oxygen and carbon atoms, respectively, showing the electrostatic repulsion drives the configuration and adsorption efficiencies. For the ternary component system, the most stable configurations were reached when all aromatic molecules adsorb parallel to the Hap surface. In such condition, besides the electrostatic effect, the mass transport phenomenon is also operative with the diffusion of Fur being favored thus implying greater availability of this molecule on Hap surface leading to its observed higher adsorption efficiency in respect to the other studied adsorbates.

Supplementary Information

Supplementary information is available free of charge at http://jbcs.sbq.org.br as a PDF file.

Acknowledgments

The authors are in debt with Dr Paula Homem-de-Melo (Universidade Federal do ABC, Santo André-SP) and Dr Sazaki (Laboratório de Raios-X, Universidade Federal do Ceará) for providing the computational resources and XRD facility, respectively. E. L. (No. 306896/2018-4) and I. C. N. D. (No. 307078/2017-5) are thankful to CNPq for the grants, CAPES and FUNCAP/PRONEX/2015 PR2-0101-00030.01.00/15 SPU No. 3265612/2015 for financial support.

References

1. http://data.consilium.europa.eu/doc/document/ST-10607-2016-INIT/en/pdf, accessed on February 16, 2019.
2. Baia, L. V.; Souza, W. C.; Souza, R. J. F.; Veloso, C. O.; Chiaro, S. S. X.; Figueiredo, M. A. G.; *Energy Fuels* **2017**, 11731.
3. Dantas, T. N. C.; Dantas Neto, A. A.; Moura, M. C. P. A.; Barros Neto, E. L.; Duarte, K. R. F.; *Braz. J. Pet. Gas* **2014**, *8*, 15.
4. Mathieu, Y.; Tzanis, L.; Soulard, M.; Patarin, J.; Vierling, M.; Molière, M.; *Fuel Process. Technol.* **2013**, *114*, 81.
5. Liu, D.; Gui, J.; Sun, Z.; *J. Mol. Catal. A: Chem.* **2008**, *291*, 17.
6. Santos, A. L.; Reis, R. A.; Rossa, V.; Reis, M. M.; Costa, A. L. H.; Veloso, C. O.; Henriques, C. A.; Zotin, F. M. Z.; Paredes, M. L. L.; Silveira, E. B.; Chiaro, S. S. X.; *Mater. Lett.* **2012**, *83*, 158.
7. Saleh, T. A.; Sulaiman, K. O.; Al-Hammadi, S. A.; Dafalla, H.; Danmaliki, G. I.; *J. Cleaner Prod.* **2017**, *154*, 401.
8. Dehghan, R.; Anbia, M.; *Fuel Process. Technol.* **2017**, *167*, 99.
9. Sun, X.; Tatarchuk, B. J.; *Fuel* **2016**, *183*, 550.
10. Sarker, M.; Yoon, J.; Rim, A.; Sik, K.; Hwa, S.; *J. Hazard. Mater.* **2018**, *344*, 593.
11. Khan, N. A.; Jhung, S. H.; *J. Hazard. Mater.* **2017**, *325*, 198.
12. Chen, Z.; Ling, L.; Wang, B.; Fan, H.; Shangguan, J.; Mi, J.; *Appl. Surf. Sci.* **2016**, *387*, 483.
13. Hernandez-Maldonado, A. J.; Yang, R. T.; *J. Am. Chem. Soc.* **2004**, *126*, 992.
14. Boisson, J.; Ruttens, A.; Mench, M.; Vangronsveld, J.; *Environ. Pollut.* **1999**, *104*, 225.
15. He, M.; Shi, H.; Zhao, X.; Yu, Y.; Qu, B.; *Procedia Environ. Sci.* **2013**, *18*, 657.

16. Mignardi, S.; Corami, A.; Ferrini, V.; *Chemosphere* **2012**, *86*, 354.
17. Ramakrishnan, P.; Nagarajan, S.; Thiruvenkatam, V.; *Appl. Clay Sci.* **2016**, *134*, 136.
18. Sandrine, B.; Ange, N.; Didier, B.-A.; Eric, C.; Patrick, S.; *J. Hazard. Mater.* **2007**, *139*, 443.
19. Lusvardi, G.; Malavasi, G.; Menabue, L.; Saladini, M.; *Waste Manage.* **2002**, *22*, 853.
20. Sena, L. A.; Caraballo, M. M.; Rossi, A. M.; Soares, G. A.; *J. Mater. Sci.: Mater. Med.* **2009**, *20*, 2395.
21. Fihri, A.; Len, C.; Varma, R. S.; Solhy, A.; *Coord. Chem. Rev.* **2017**, *347*, 48.
22. Smiciklas, I.; Dimovic, S.; Plecas, I.; Mitric, M.; *Water Res.* **2006**, *40*, 2267.
23. Vieira, E. G.; Vieira, T. W. S.; Silva, M. P.; Santos, M. V. B.; Brito, C. A. R. S.; Bezerra, R. D. S.; Fialho, A. C. V.; Osajima, J. A.; Silva Filho, E. C. In *Biomaterials*; Pignatello, R., ed.; IntechOpen: London, UK, 2018, p. 87.
24. Campisi, S.; Castellano, C.; Gervasini, A.; *New J. Chem.* **2018**, *42*, 4520.
25. Zhou, J.; Tsao, H.; Sheng, Y.; Jiang, S.; *J. Chem. Phys.* **2004**, *121*, 1050.
26. Neves, R. S.; Motheo, A. J.; Fernandes, F. M. S. S.; Fartaria, R. P. S.; *J. Braz. Chem. Soc.* **2004**, *15*, 224.
27. Liu, J.; Monson, P. A.; *Ind. Eng. Chem. Res.* **2006**, *45*, 5649.
28. Ghalami, Z.; Ghoulipour, V.; Khanchi, A.; *Appl. Surf. Sci.* **2019**, *471*, 726.
29. Liao, C.; Xie, Y.; Zhou, J.; *RSC Adv.* **2014**, *4*, 15759.
30. Andrade Neto, D. M.; Carvalho, E. V.; Rodrigues, E. A.; Feitosa, V. P.; Sauro, S.; Mele, G.; Carbone, L.; Mazzetto, S. E.; Rodrigues, L. K.; Fechine, P. B. A.; *Dent. Mater.* **2016**, *32*, 784.
31. American Public Health Association (APHA), American Water Works Association (AWWA), Water Environment Federation (WEF); *Standard Methods for the Examination of Water and Wastewater*, 21st ed.; American Public Health Association: Washington D.C., 2005.
32. Brunauer, S.; Emmett, P.; Teller, E.; *J. Am. Chem. Soc.* **1938**, *60*, 309.
33. Fletcher, R.; *Practical Methods of Optimization*, vol. 1; John Wiley & Sons: New York, 1980.
34. Becke, A. D.; *J. Chem. Phys.* **1993**, *98*, 1372.
35. Lee, C.; Yang, W.; Parr, R. G.; *Phys. Rev. B* **1988**, *37*, 785.
36. Frisch, M. J.; Trucks, G. W.; Schlegel, H. B.; Scuseria, G. E.; Robb, M. A.; Cheeseman, J. R.; Scalmani, G.; Barone, V.; Mennucci, B.; Petersson, G. A.; Nakatsuji, H.; Caricato, M.; Li, X.; Hratchian, H. P.; Izmaylov, A. F.; Bloino, J.; Zheng, G.; Sonnenberg, J. L.; Hada, M.; Ehara, M.; Toyota, K.; Fukuda, R.; Hasegawa, J.; Ishida, M.; Nakajima, T.; Honda, Y.; Kitao, O.; Nakai, H.; Vreven, T.; Montgomery Jr., J. A.; Peralta, J. E.; Ogliaro, F.; Bearpark, M.; Heyd, J. J.; Brothers, E.; Kudin, K. N.; Staroverov, V. N.; Kobayashi, R.; Normand, J.; Raghavachari, K.; Rendell, A.; Burant, J. C.; Iyengar, S. S.; Tomasi, J.; Cossi, M.; Rega, N.; Millam, J. M.; Klene, M.; Knox, J. E.; Cross, J. B.; Bakken, V.; Adamo, C.; Jaramillo, J.; Gomperts, R.; Stratmann, R. E.; Yazyev, O.; Austin, A. J.; Cammi, R.; Pomelli, C.; Ochterski, J. W.; Martin, R. L.; Morokuma, K.; Zakrzewski, V. G.; Voth, G. A.; Salvador, P.; Dannenberg, J. J.; Dapprich, S.; Daniels, A. D.; Farkas, Ö.; Foresman, J. B.; Ortiz, J. V.; Cioslowski, J.; Fox, D. J.; *Gaussian 09, Revision A1*, Gaussian, Inc.: Wallingford, CT, 2009.
37. Obot, I. B.; Macdonald, D. D.; Gasem, Z. M.; *Corros. Sci.* **2015**, *99*, 1.
38. Houk, K. N.; *J. Am. Chem. Soc.* **1973**, *95*, 4092.
39. Dunnington, B. D.; Schmidt, J. R.; *J. Catal.* **2015**, *324*, 50.
40. Janak, J. F.; *Phys. Rev. B* **1978**, *18*, 7165.
41. Koopmans, T.; *Physica* **1934**, *1*, 104.
42. Binder, K.; Heermann, D.; Roelofs, L.; Mallinckrodt, A. J.; McKay, S.; *Comput. Phys.* **1993**, *7*, 156.
43. Akkermans, R.; Spenley, N.; Robertson, S.; *Mol. Simul.* **2013**, *39*, 1153.
44. Fleet, M.; Liu, X.; King, P.; *Am. Mineral.* **2004**, *89*, 1422.
45. Mayo, S.; Olafson, B.; Goddard, W.; *J. Phys. Chem.* **1990**, *94*, 8897.
46. Koutsopoulos, S.; *J. Biomed. Mater. Res.* **2002**, *62*, 600.
47. Sing, K.; *Pure Appl. Chem.* **1982**, *54*, 2201.
48. El-Shafei, G. M. S.; Philip, C. A.; Moussa, N. A.; *J. Colloid Interface Sci.* **2004**, *277*, 410.
49. Scudeller, L. A.; Mavropoulos, E.; Tanaka, M. N.; Costa, A. M.; Braga, C. A. C.; López, E. O.; Mello, A.; Rossi, A. M.; *Mater. Sci. Eng., C* **2017**, *79*, 802.
50. Wu, Y.; Bose, S.; *Langmuir* **2005**, *1*, 3232.
51. Wu, F.-C.; Tseng, R.-L.; Juang, R.-S.; *Chem. Eng. J.* **2009**, *153*, 1.
52. Pearson, R. G.; *J. Am. Chem. Soc.* **1963**, *85*, 3533.
53. Yang, R. T.; *Adsorbents: Fundamentals and Applications*; John Wiley & Sons, Inc.: Hoboken, 2003.
54. Guo, L.; Obot, I. B.; Zheng, X.; Shen, X.; Qiang, Y.; Kaya, S.; Kaya, C.; *Appl. Surf. Sci.* **2017**, *406*, 301.
55. Harja, M.; Ciobanu, G.; *Sci. Total Environ.* **2018**, *628-629*, 36.
56. Guo, H.; Jiang, C.; Xu, Z.; Luo, P.; Fu, Z.; Zhang, J.; *Mater. Lett.* **2019**, *241*, 176.
57. Krukowski, S.; Karasiewicz, M.; Lysenko, N.; Kolmas, J.; *Colloids Surf., A* **2018**, *558*, 23.

Submitted: February 22, 2019
Published online: June 26, 2019